CHARACTERIZATION OF SHEET METAL FOR THE AUTOMOTIVE INDUSTRY

Tânia F. Madeira

Instituto Superior Técnico, University of Lisbon, Portugal
E-mail: tania.madeira@tecnico.ulisboa.pt

Abstract

The increasing technological development of the automotive industry aims for a continuous search of materials with better properties and quality, enabling the possibility of acquiring products with lower costs, increasing the vehicle efficiency and the quality/price ratio. Knowledge of the mechanical properties and formability limits of necking and fracture become central to assess the suitability of different materials to several forming processes.

This work has two main objectives, the first one was to characterize mechanically three metal alloys, which include an aluminium alloy AA5182, an alloy steel DP500 and an alloy steel DC04 with different thicknesses (0.6 mm and 1 mm) by estimating their mechanical properties by a tensile test. The determination of the formability limits was also performed by means of tensile, bulge and SPIF tests. The fracture toughness was also characterized for the aluminium alloy AA1050-H111 and alloy steel DC04 (0.6 mm) using double notch test specimens under tension.

The second objective was to analyses the fracture in truncated conical and pyramidal SPIF parts giving a new contribute to the understanding of plastic deformation and fracture mechanics of sheet metal.

A comparative analysis between the different materials was carried out throughout the study while also being performed a comparison for the same material (DC04) with different thicknesses in order to understand the influence of the thickness in the formability.

Keywords: Aluminium, Steel, formability limits, Forming limit curve (FLC), Fracture forming curve (FFL), Single point incremental forming (SPIF).

1. Introduction

Formability is the term usually used to characterize the maximum plastic deformation that can be achieved during a technological process without the occurrence of necking or fracture. There are two formability limits: by necking, characterized by a “V-shaped” curve which is designated as the forming limit curve (FLC), and by fracture. If the fracture limit is associated with tensile stresses is governed by the fracture forming limit (FFL), whereas if the fracture limit is associated with in-plane shear stresses is governed by the shear fracture forming limit (SFFL).

The forming limit curve (FLC) is a graphical representation in the principal strains plane, which can be divided in two regions: the region below the curve that corresponds to the allowable deformations and the region above the curve that corresponds to the non-admissible deformations, or when necking occurs. The fracture forming limit line (FFL) is a graphical representation of the instant in which the fracture occurs, originally proposed by Atkins [1] and it’s characterized by a straight line falling from left to right with a slope equal to “−1” associated to the condition of critical thickness reduction at failure caused by tension (mode I of fracture mechanics, see Figure 1a). Isik et al. [2] introduced the SFFL and represented it in the principal strains space as a perpendicular straight line to FFL in fair agreement with the condition of critical distortion at fracture induced by in-plane shear (mode II of fracture mechanics, see Figure 1b).

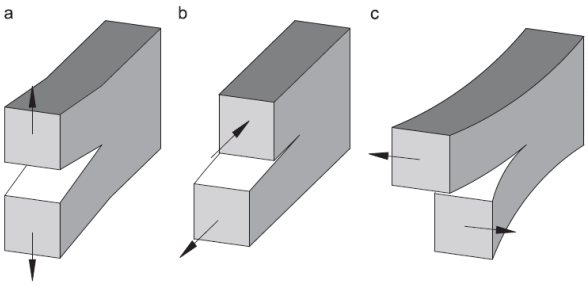

Figure 1 The three crack separation modes: a. Mode I – tensile stresses, b. Mode II – in-plane shear stresses and c. Mode III – out-of-plane shear stresses [3].

The formability testing methods based on forming limit diagrams can be classified as uniaxial, plane-strain and biaxial formability tests as a function of the deformation mode, considering the strain loading path that is characteristic of each specific test.

Authors propose a new methodology to determine the formability limits by fracture in the principal strain space. The methodology is based on experimental tests performed in single point incremental forming (SPIF) of truncated conical and pyramidal geometries with varying drawing angles, torsion and plane shear specimens. Special emphasis is placed on the determination of the FFL by means of SPIF tests because, contrary to commonly utilized methods and procedures for constructing the FLC, the proposed methodology will not make use of conventional sheet metal formability tests to obtain the experimental values of strains at fracture [2].

2. EXPERIMENTATION

This investigation concerns to the mechanical and formability characterization, in which was used four different materials: aluminium alloy AA1050-H111 with 1 mm in thickness, aluminium alloy AA5182 with 1 mm in thickness, steel DP500 with 0.62 mm in thickness and steel DC04 with 1mm and 0.6 mm, were used. As mechanical tests, were carried out the tensile tests. As formability tests were performed tensile, Bulge and SPIF tests.

2.1. Mechanical and formability characterization

The experimental work was performed on four different materials and the mechanical characterization of the material was performed by means of tensile tests in specimens that were cut out from the supplied sheets at 0º, 45º and 90º with respect to the rolling direction.

The modulus of elasticity E, the yield strength, σ_y, the ultimate tensile strength, σ_{UTS}, the anisotropy coefficient, r and the elongation at break, A, at 0º, 45º and 90º with respect to the rolling direction (RD). The normal $\bar{r}$ and planar Δr anisotropy coefficients were determined from,

$$\bar{r} = \frac{(r_0 + 2r_{45} + r_{90})}{4} \qquad \Delta r = \frac{r_0 + r_{90} - 2r_{45}}{2} \tag{1}$$

The methodology used for determining the FLC was based upon measuring the in-plane strains (ε_1,ε_2) from grid points along predefined directions crossing the crack perpendicularly. The procedure involved interpolation of the experimental in-plane strains into a 'bell-shaped curve' in order to reconstruct the distribution of strains in the area of intense localization and subsequent extrapolation of the maximum strain pairs at the onset of necking. The in-plane strains (ε_1,ε_2) at the grid points were obtained as follows,

$$\varepsilon_1 = \ln\left(\frac{a}{d}\right) \qquad \varepsilon_2 = \ln\left(\frac{b}{d}\right) \tag{2}$$

where a and b are the lengths of the major and minor axes of the ellipses that resulted from plastic deformation of the original grid of overlapping circles during sheet formability tests. In contrast, the methodology used for determining the FFL was based upon measuring the thickness of the specimens

before and after fracture at several locations along the crack in order to obtain the 'gauge length' strains. The measurements were performed in a minimum of two specimens taken from the fractured area. A compact inverted metallurgical microscope (Olympus CK40M) was utilized with x10 magnification.

These strains were subsequently fitted by a straight line falling from left to right in fair agreement with the theoretical conditions of critical thickness reduction $r_{máx}$ at fracture (slope '−1').

2.2. Fracture toughness from SPIF tests

The procedure employed for determining fracture toughness in truncated conical SPIF parts considers plastic work W that makes up the specific work at fracture (also known as fracture toughness, R) to be dissipated in thin boundary layers of thickness h alongside the crack surfaces (Figure 2),

$$W = \left(\int_0^{\bar{\varepsilon}_f} \bar{\sigma}\, d\bar{\varepsilon} \right) h dA \tag{3}$$

where dA is the increase in crack area, $h\,dA$ is the associated increase in volume according to Atkins and Mai [5], $\bar{\sigma}$ is the effective stress and $\bar{\varepsilon}$ is the effective strain. The effective strain at fracture $\bar{\varepsilon}_f$ is obtained from the experimental values of strain $(\varepsilon_{1f}, \varepsilon_{2f}, \varepsilon_{3f})$ in the meridional, circumferential and thickness directions according to the anisotropic yield criterion due to Hill [6],

$$\bar{\varepsilon}_f = \frac{1+r}{\sqrt{(1+2r)}} \sqrt{\varepsilon_{1f}^2 + \varepsilon_{2f}^2 + \frac{2r}{(1+r)} \varepsilon_{1f} \varepsilon_{2f}} \tag{4}$$

Because fracture toughness R is defined by

$$w = \frac{W}{A} = \frac{W_p}{A} + \frac{W_s}{A} = \frac{W_p}{A} + R \tag{5}$$

as the work per unit of area w_s that is needed to create a new surface, its value can be determined by dividing the plastic work W in equation (3) by the increase in crack area dA,

$$R = h \int_0^{\bar{\varepsilon}_f} \bar{\sigma}\, d\bar{\varepsilon} \cong t \int_0^{\bar{\varepsilon}_f} \bar{\sigma}\, d\bar{\varepsilon} \tag{6}$$

where the approximation in equation (6) results from taking the thickness h of the boundary layer as the deformed sheet thickness t as it was suggested by Atkins and Mai [5] in their work on fracture toughness in sheet metal forming.

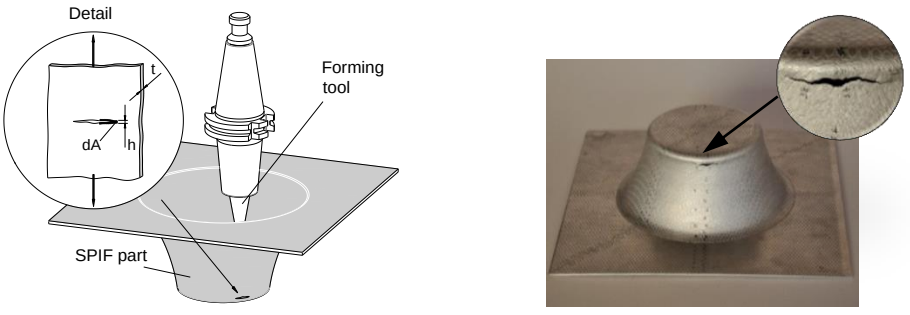

(a) (b)

Figure 2 Determining fracture toughness directly from SPIF tests (a) Circumferential crack with notation and detail showing the hatched region corresponding to a thin boundary layer alongside the crack; (b) Truncated conical part fabricated by SPIF with a detail of a circumferential [4].

In physical terms the assumption that the boundary layer h alongside the crack surface is of the order of magnitude of the deformed sheet thickness t is justified by the significant and uniform reduction of

the initial sheet thickness t_0 (sometimes above 70%) that is commonly observed in SPIF parts namely in truncated conical SPIF parts.

Now, by taking into consideration that truncated conical SPIF parts undergo plastic deformation along proportional $\beta = d\varepsilon_2/d\varepsilon_1 = \varepsilon_2/\varepsilon_1$, plane strain loading conditions and bearing in mind that the effective stress $\overline{\sigma}$ is calculated from the experimental values of the effective strain $\overline{\varepsilon}$, it is possible to determine fracture toughness R directly from the experimental values of effective strain at fracture, as follows,

$$R \cong t \int_0^{\overline{\varepsilon}_f} K\varepsilon^n \, d\overline{\varepsilon} = t \, \frac{K\overline{\varepsilon}_f^{\,n}}{n+1} \tag{7}$$

2.3. Plan of experiments

The table 1 show the plane of experiments for different materials with information about the material used, the thickness of the sheet metal, the type of test, the dimension of specimens and the number of tests.

Table 1 – Plane of experiments for the materials.

Material	Thickness (mm)	Test	Dimension of specimens	Number of tests
AA1050-H111	1	Double notched	5, 10, 15, 20 e 25	20
	1.5			20
	2			20
AA5182	1	Tensile	$l_0 = 50$	12
			$l_0 = 80$	15
		Bulge	Ø 100	3
			100:90	2
			100:80	2
			100:64	2
		SPIF	Conical	2
			Pyramidal	2
DC04	1	Tensile	$l_0 = 50$	12
			$l_0 = 80$	15
		Bulge	Ø 100	3
			100:90	2
			100:80	2
			100:64	2
		SPIF	Conical	2
			Pyramidal	2
DC04	0.6	Tensile	$l_0 = 50$	15
		Bulge	Ø 100	3
			100:90	4
			100:80	4
			100:64	4
		SPIF	Conical	2
			Pyramidal	2
		Double notched	7.5, 12.5, 15, 20 e 25	20
DP500	0.62	Tensile	$l_0 = 50$	12
			$l_0 = 80$	15
		Bulge	Ø 100	3
			100:90	2
			100:80	2
			100:64	2
		SPIF	Conical	2
			Pyramidal	2
Total of specimens				**234**

3. RESULTS AND DISCUSSION

3.1. Mechanical Characterization

The mechanical characterization of materials was performed by tensile tests, at room temperature, and the average stress-strain curve was approximated by the several Ludwik-Hollomon's equations (see Table 2).

Table 2 – Ludwik-Hollomon's equation for different materials

	$l_0 = 50\ mm$	$l_0 = 80\ mm$
AA5182	$\sigma = 618\varepsilon^{0.33}\ (MPa)$	$\sigma = 571\varepsilon^{0.33}\ (MPa)$
DP500	$\sigma = 1062\varepsilon^{0.23}\ (MPa)$	$\sigma = 1061\varepsilon^{0.22}\ (MPa)$
DC04 (1 mm)	$\sigma = 620\varepsilon^{0.20}\ (MPa)$	$\sigma = 627\varepsilon^{0.23}\ (MPa)$
DC04 (0.6mm)	$\sigma = 574\varepsilon^{0.22}\ (MPa)$	-

Table 3 presents the main properties obtained by performing tensile tests for materials chosen for 0º, 45° and 90° relative to the rolling direction.

Table 3 - Summary of the mechanical properties of different materials.

Material	l_0 (mm)	Modulus of elasticity, E (GPa)	Yield Strength, σ_e (MPa)		Ultimate tensile strength, σ_r (MPa)	Elongation at break, A (%)	Anisotropy coefficient
AA5182	50	70.8	157.6 (min)	154.7 (min)	370.3	25.0	$\bar{r} = 0.72$ $\Delta r = 0.02$
	80	64.7	144.3 (máx)	139.4 (máx)	336.1	25.4	$\bar{r} = 0.80$ $\Delta r = 0.10$
DP500	50	199.4	302.6		685.4	25.2	$\bar{r} = 0.86$ $\Delta r = -0.09$
	80	200.4	316.9		688.7	25.6	-
DC04 (1 mm)	50	208.6	225.0		467.8	40.0	$\bar{r} = 1.22$ $\Delta r = 0.54$
	80	183.4	207.9		439.2	37.8	$\bar{r} = 1.28$ $\Delta r = -0.03$
DC04 (0.6 mm)	50	210.2	179.4		417.3	45.3	$\bar{r} = 1.88$ $\Delta r = 0.79$

3.2. Fracture toughness characterization

The procedure for determining fracture toughness in crack opening mode I is based on double edge notched test specimens loaded in tension. In fact, by taking into consideration the experimental evolutions of the tensile force with displacement in double edge notched test specimens with different ligaments c = 5, 10, 15, 20, 25 mm for 1 mm of thickness and c = 7.5, 12.5, 15, 20, 25 mm for 1.5 mm and 2 mm of thickness that are shown in Figure 3 (only for 1 mm because the other results are similar) it is possible to conclude that the amount of energy per unit of area to create a new surface (fracture toughness) is equal to R = 56.9 kJ/m^{2,} R = 89.7 kJ/m^2 and R = 105.8 kJ/m^2, respectively. These values of fracture toughness are an average value that results from double edge notched test specimens that were cut out from the supplied sheets at 0º and 90º degrees with respect to the rolling direction (refer to Table 4).

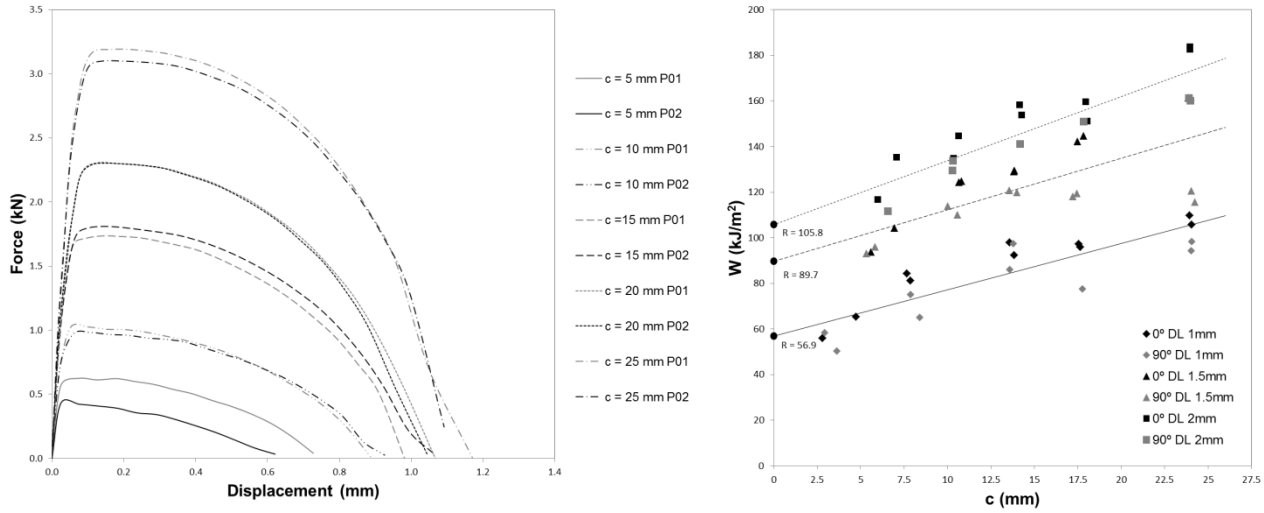

Figure 3 Fracture toughness in aluminium AA1050-H111 sheets with 1 mm thickness obtained from double edge notched test specimens loaded in tension. (a) Experimental evolution of the tensile force with displacement for test specimens with different ligaments that were cut out from the supplied sheets at 0º with respect to the rolling direction; (b) Average value of fracture toughness obtained from test specimens with different ligaments that were cut out from the supplied sheets at 0º and 90º with respect to the rolling direction.

The determination of the fracture toughness values ware also made for mild steel DC04 for the same method and the results are shown in Table 4.

Table 4 Fracture toughness, R, obtained from double edge test specimens loaded in tension that were cut out from the supplied sheets at 0º and 90º degrees with respect to the rolling direction.

Material	Thickness (mm)	0º DL	90º DL	Average
AA1050-H111	1.0	60.2	53.6	**56.9**
	1.5	82.2	96.4	**89.7**
	2.0	106.4	102.6	**105.8**
DC04	0.6	216.24	208.03	**212.14**

3.3. Formability Limits

The FLC was determined combining tensile tests and bulge tests. It was constructed by measuring the in-plane strains (ε_1,ε_2) from grid points located along predefined directions crossing the crack perpendicularly and a procedure that involves the interpolation of these strains. The resulting FLC's are shown in Figure 4 for different materials.

The determination of the FFL is different from the determination of the FLC. Application of grids, even with very small circles in order to obtain strains in the necking region after it forms and, therefore, close to the fracture, provides strain values that cannot be considered the fracture strains. Moreover, such grids create measurement problems and suffer from sensitivity to the initial size of the circles used in the grids due to the inhomogeneous deformation in the neighbourhood of the crack. As a result of this, to obtain the FFL's of the different materials sheet blanks the technique used required measuring thickness and width before and after fracture in a microscope, at several places along the crack, in order to obtain the 'gauge length' strains.

The FFL was determined by combining the fracture in-plane strain pairs measured from SPIF tests on truncated conical and pyramidal geometries with the 'gauge length' strains (strains along thickness direction). The FFL for the studied materials can be defined by the equations in Table 5. In Figure 4 the light grey areas around the FFL correspond to uncertainty intervals of 10% associated to experimental errors during the determination of these limits.

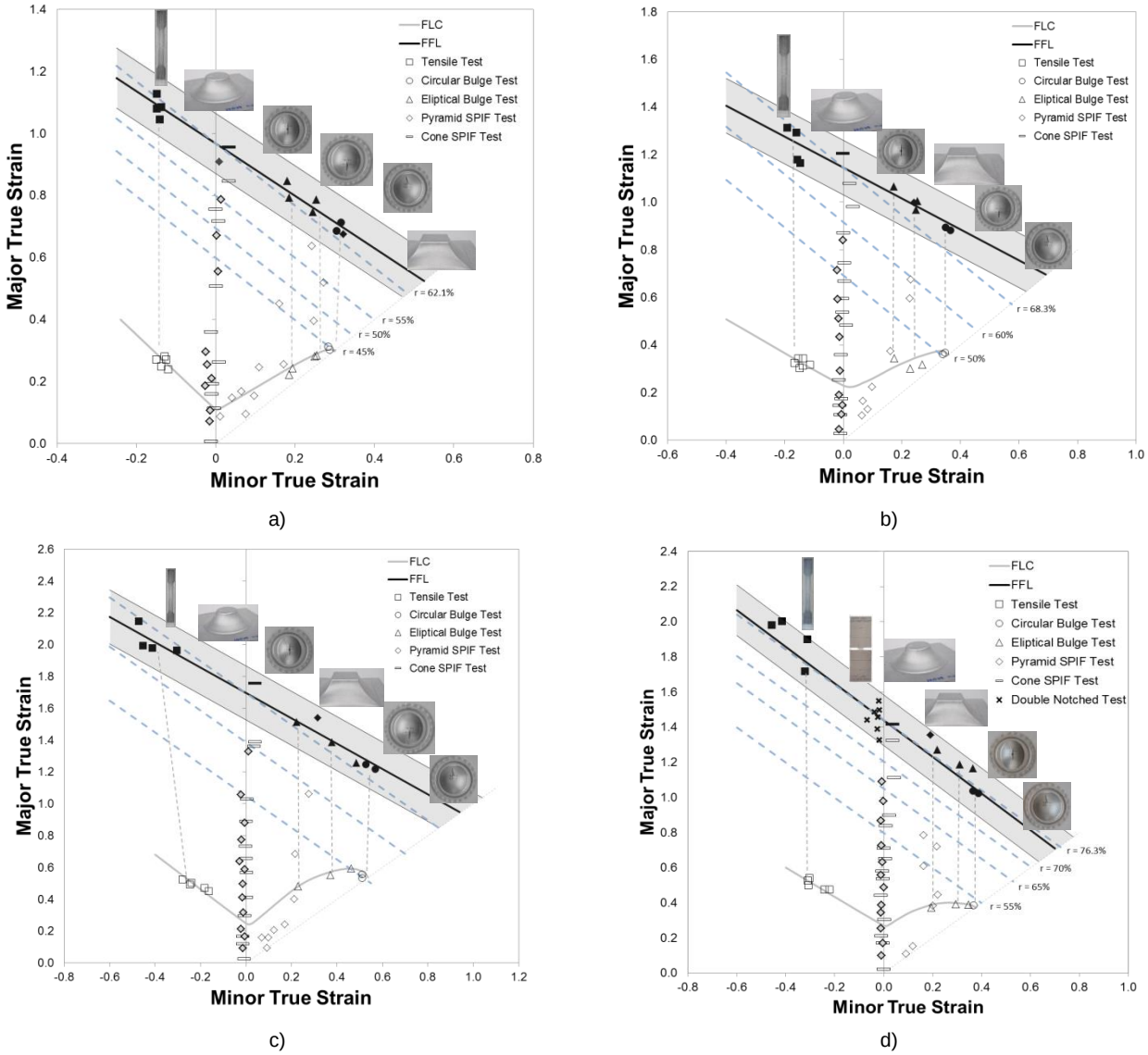

Figure 4 - Forming limit curve (FLC) and fracture forming line (FFL) of the a) AA5182, b) DP500, c) DC04 (1 mm) and d) DC04 (0.6mm) in the principal strain space.

The resulting FFL's (Table 5) are in good agreement with the condition of constant thickness strain at fracture due to Atkins [1], where the reduction in sheet thickness at the onset of failure by fracture were show in Table 5 (refer to the dashed upper blue line in Figure 4). The distance between FLC and FFL was calculated in order to identify the material that presented the best behaviour under plane strain conditions ($\Delta\boldsymbol{\varepsilon_1}$).

Table 5 Equations which determines the FFL, reduction of thickness ($r_{máx}$) and distance between FLC e FFL ($\Delta\boldsymbol{\varepsilon_1}$).

	FFL	$r_{máx}$	$\Delta\boldsymbol{\varepsilon_1}$
AA5182	$\varepsilon_1 + 0.84\varepsilon_2 = 0.97$	62.1%	0.64
DP500	$\varepsilon_1 + 0.65\varepsilon_2 = 1.15$	68.3%	0.92
DC04 (1 mm)	$\varepsilon_1 + 0.80\varepsilon_2 = 1.70$	81.7%	1.5
DC04 (0.6 mm)	$\varepsilon_1 + 1.04\varepsilon_2 = 1.44$	76.3%	1.22

3.4. Single Point Incremental Forming

In this paper was proposed to make a contribution to the work previously performed by Silva et al. [7], who studied the influence of the tool radius in SPIF test for aluminum alloy AA1050-H111. The work allowed identifying a critical threshold for the ratio between the thickness of the sheet and the radius of the tool that distinguishes between fracture with and without previous necking. The extensions are only measures the surface of the plate. The mechanical properties were previously determined by Cristino, et al. [8].

The major and minor experimental true strains in the principal strain space that were obtained from SPIF tests were performed with different tool radius r_{tool} in order to change the ratio r_{part}/r_{tool} between the radius r_{part} of the part and the radius r_{tool} of the forming tool was show in Figure 5.

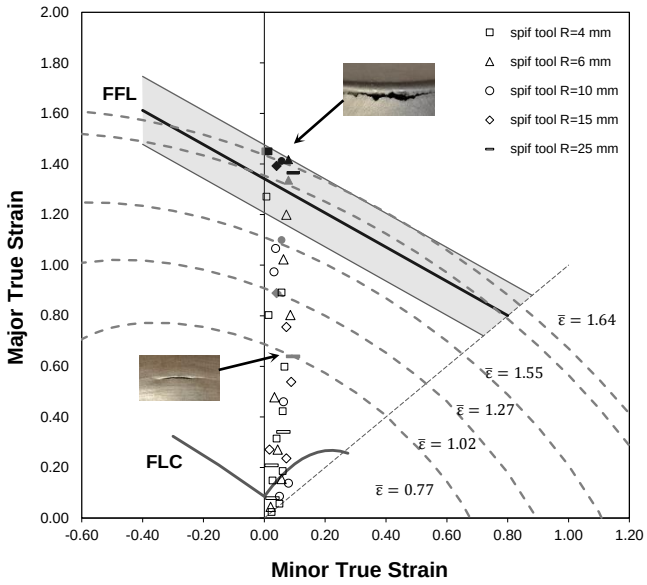

Figure 5 - Experimental strains obtained from SPIF tests performed with five different hemispherical-ended tools. The grey solid marks refer to the strain pairs at the onset of necking, the black solid marks refer to the strain pairs at the onset of fracture and the elliptical dashed grey curves refer to the iso-effective strain contours.

The experimental strain loading paths in Figure 5 indicate that truncated conical SPIF parts are formed under plane strain conditions and allow concluding that grey solid markers, corresponding to the tests performed with hemispherical-ended tools of radius $\mathrm{r_{tool}} = 4 \text{ and } 6\ \mathrm{mm}$, are in agreement with the FFL. In contrast, the grey solid markers corresponding to the tests performed with hemispherical-ended tools of radius $\mathrm{r_{tool}} = 10, 15 \text{ and } 25\ \mathrm{mm}$ are located in-between the FLC and the FFL, getting closer to the FLC as the tool radius $\mathrm{r_{tool}}$ increases.

The overall set of results corroborates the influence of the ratio r_{tool} on the physics of failure and proves that large values of r_{part}/r_{tool} and small tool radius r_{tool} lead to failure by fracture with suppression of necking whereas small values of r_{part}/r_{tool} and large tool radius tool r lead to failure by fracture with previous necking. Moreover, results also show that in case of necking, the onset of failure is delayed by the stabilizing effects induced by dynamic bending under tension that are controlled by the ratio t/r_{tool} between the sheet thickness *t* and the radius r_{tool} of the forming tool.

The black solid markers in Figure 5 show the fracture strain pairs obtained from the 'gauge length' strains. As seen in the figure 6, the limiting strain pairs at fracture are identical for all the test cases performed with the five different hemispherical-ended tools and their values are consistent with the FFL that had been previously determined from sheet formability tests. This result corroborates Silva et al. [7] vision that SPIF fails by fracture with suppression of necking for large values of r_{part}/r_{tool} and small r_{tool} due to closeness of grey and black solid markers in case of tests performed with hemispherical-ended tools of radius $r_{tool} = 4 \;\; and \; 6 \; mm$.

In relation to the value of fracture toughness from the SPIF test was calculated only for the sheet thickness of 1 mm and obtained by the procedure described in the session 2.2. The equation 7 provides a simple and effective procedure to determine fracture toughness *R* from the black solid markers in Figure 5 without the necessity of integrating the strains and stresses along the loading path. In fact, by replacing the effective strain $\bar{\varepsilon} = 1.64$ retrieved from the iso-effective strain contour plotted in Figure 6 it is possible to determine an experimental value of fracture toughness *R* = 52.0 kJ/m^2.

If, in addition to the similarity between the two estimates of fracture toughness (52.0 and 56.89 kJ/m^2), one considers the work of Muscat-Fenech et al. [9] who were able to correlate the FFL with fracture toughness in mode I it is straightforward to conclude that failure by fracture in SPIF occurs by opening mode I due to the meridional stresses that are applied along the plastically deforming region resulting from the contact between the sheet and the forming tool. This is further justified by the circumstance that fracture strain pairs of the truncated conical parts that fail by circumferential cracking due to meridional tensile stresses are located very close to the iso-fracture toughness contour of the fracture strain pairs that were determined from the double notched test specimens loaded in tension that fail by cracking in opening mode I (Figure 6).

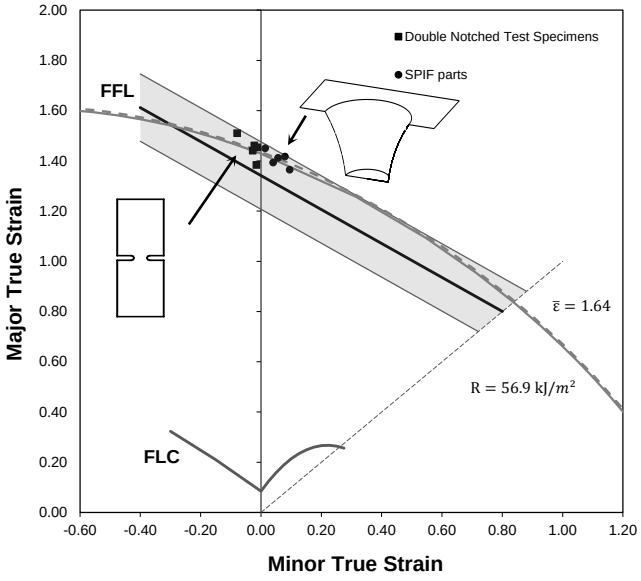

Figure 6 Fracture strain pairs obtained from measurements in SPIF parts and double notched test specimens loaded in tension. The elliptical dashed and solid grey curves refer to the iso-effective strain and iso-fracture toughness contours, respectively.

4. Conclusions

From the mechanical properties obtained in this thesis work, it is possible to conclude that the steel DC04 was the material with better formability.

DC04 steel is the material that has the greatest distance between FLC and FFL (see Table 5). Thus, it is concluded that the steel alloy DC04 presents itself as a material extremely ductile allowing a considerable degree of extension in the thickness direction between the onset of necking and fracture, while the steel alloy DP500 and aluminium alloy AA5182 show a lightly ductile behaviour.

Results show the importance of measuring thickness before and after fracture along the cracks in order to obtain the 'gauge length' fracture strain pairs and to ensure compatibility with the fracture forming limit line (FFL) no matter which r_{part}/r_{tool}. This procedure avoids scattering of the limiting strain pairs and deviations from both the forming limit curve (FLC) and the FFL when strains are retrieved from conventional circle grid analysis on test cases performed with different values of r_{part}/r_{tool} and r_{tool}.

Determination of fracture toughness directly from truncated conical and pyramidal truncated SPIF parts at failure and from independent double notched test specimens loaded in tension allow concluding that plastic flow and failure for these geometries are typical of crack opening mode I under meridional tensile stresses.

References

[1] Atkins, A.G. (1996), Fracture in forming, *Journal of Materials Processing Technology*, 56, 609-618.

[2] Isik, K., Silva, M.B., Tekkaya, A.E., Martins, P.A.F. (2014), Formability limits by fracture in sheet metal forming. *Journal of Materials Processing Technology*. 214, 1557–1565.

[3] Martins, P.A.F., Bay, N., Tekkaya, A. E., Atkins, A. G. (2014), Characterization of fracture loci in metal forming, International Journal of Mechanical Sciences. 83, 112-123.

[4] Madeira, T., Silva, C. M. A., Silva, M. B., Martins, P. A. F. (2014), Failure in Single Point Incremental Forming, International Journal of Advanced Manufacturing Technology, aceite para publicação.

[5] Atkins A.G., Mai Y.W. (1985) Elastic and plastic fracture: metals, polymers, ceramics, composites, biological materials. Ellis Horwood, Chichester, UK

[6] Hill R. (1948) A theory of yielding and plastic flow of anisotropic metals. Proceedings of the Royal Society of London (Series A) 193: 281-297

[7] Silva, M.B., Nielsen, P.S., Bay, N., Martins, P.A.F. (2011). Failure mechanisms in single point incremental forming of metals. *International Journal of Advanced Manufacturing Technology*. 56, 893–903

[8] Cristino V. A. M., Montanari L., Silva M. B., Martins P. A. F. (2014), Towards square hole-flanging produced by single point incremental forming, *Journal of Materials: Design and Applications,* 0(0), 1-9.

[9] Muscat-Fenech CM, Arndt, S, Atkins AG (1996) The determination of fracture forming limit diagrams from fracture toughness. 4th International Sheet Metal Conference, University of Twente, The Netherlands 1: 249-260.